PCCP

PAPER

View Article Online
View Journal | View Issue

Cite this: *Phys. Chem. Chem. Phys.*, 2025, **27**, 14379

Rational molecular design of two-photon activated temoporfin: a computational study for advanced photodynamic therapy†

Basak Koca Fındık, [ab] Ege Su Uyar,[ac] Antonio Monari *[b] and Saron Catak *[a]

Photodynamic therapy (PDT) is a promising, non-invasive cancer treatment that relies on the activation of photosensitizers (PSs) by suitable light to produce cytotoxic reactive oxygen species. However, the efficiency of PDT is often hindered by the limited penetration of visible light into tissues, requiring the use of an infrared activable PS. Furthermore, PSs are usually prone to aggregation and present solubility issues limiting their bioavailability. In this study, we explore the functionalization of temoporfin (mTHPC), a clinically approved second-generation PS, with two-photon absorption (TPA) chromophores to enhance its efficiency in deep tissues. Three TPA-temoporfin conjugates (DTP1-mTHPC, DTP2-mTHPC, and DPP-mTHPC) have been designed and their properties have been investigated using a combination of quantum mechanics (QM), molecular dynamics (MD), and hybrid QM/MM simulations. Computational analysis revealed that the TPA cross section (σ) of the parent DTP moieties significantly increase when anchored to mTHPC, thus allowing efficient absorption in the near-infrared (NIR) region. Additionally, we have shown that their encapsulation with β-cyclodextrins (β-CDs) improved solubility and prevented aggregation without altering the optical properties of the PS. Simulations in a biological membrane model confirmed favorable interactions and localization of the candidate PDT agents within lipid bilayers, supporting their potential for enhanced clinical applications. This study demonstrates that rational molecular design can improve both the optical properties and the drug-delivery proficiency of temoporfin, paving the way for more effective deep-tissue PDT treatments.

Received 12th May 2025,
Accepted 9th June 2025

DOI: 10.1039/d5cp01775k

rsc.li/pccp

Introduction

Although it has been known since antiquity, the use of light in clinical applications has significantly evolved in modern practices. Phototherapy approaches correlate with the limitation of adverse side effects and, thus, globally improve the patients' quality of life. Among the different flavors of phototherapy, photodynamic therapy (PDT)[1–4] deserves particular attention owing to its widespread use and efficiency.

PDT is a method of treatment taking advantage of the irradiation of a photosensitizer with a specific wavelength of light, which is then able to produce cytotoxic species, such as singlet oxygen, $^1O_2$, which in turn induce cell death.[2,5,6] Light-activated drugs offer a non-invasive and more localized treatment option compared to alternatives, such as chemotherapy. In PDT, the PS is usually administered directly and systemically into the patient's bloodstream.[7] Then, the target tumorous area is irradiated with light of a specific wavelength enabling the excitation of the PS molecule to its singlet excited state manifold. The favorable route to generate singlet oxygen involves the long-lived population of the first triplet excited state (T_1) *via* intersystem crossing (ISC).[8,9] The persistent population of the triplet state allows the spin-allowed energy transfer with the ground state triplet oxygen, $^3O_2$, resulting in the production of $^1O_2$ and the relaxation of the PS to its singlet ground state. As the transition from $T_1 \rightarrow S_0$ is a spin-forbidden process, the T_1 states are usually longer lived, and this time interval is enough for the photosensitizer to transfer its energy to the molecular oxygen ($^3O_2$) in its proximity. The general mechanism behind the PDT process is illustrated in Fig. 1.

Even though PDT offers a non-invasive and sustainable process, its main challenges are linked to deep tissue penetration and selective targeting of cancer cells. Conceptually, an

[a] *Bogazici University, Department of Chemistry, 34342Bebek, Istanbul, Turkey. E-mail: saron.catak@bogazici.edu.tr*
[b] *Université Paris Cité and CNRS, ITODYS, F-75006, Paris, France. E-mail: antonio.monari@u-paris.fr*
[c] *University of Utah, Department of Chemistry, Salt Lake City, 84112, Utah, USA*

† Electronic supplementary information (ESI) available: ground singlet state (S_0) and first excited singlet state (S_1) geometries, QM functional performance, electronic structure calculations at the QM level, PS molecules within the biological environment including RMSD graphs, PS molecules interacting with membrane components, and encapsulated PS molecules with β-cyclodextrin units. See DOI: https://doi.org/10.1039/d5cp01775k

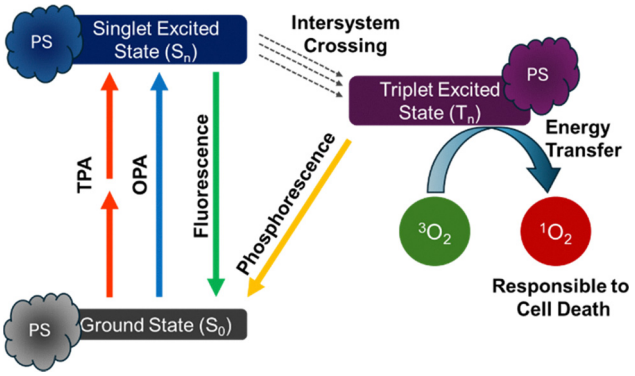

Fig. 1 PDT mechanism of action.

ideal PS should be delivered to the target tumor cells to increase treatment selectivity and also to reduce side-effects.[10] In fact, the coupling of PSs with ligands targeting receptors overexpressed in cancer cells, such as folate acid, has been of particular interest recently.[11–13] While visible light can only be used on superficial or accessible lesions, due to its limited penetration, the development of PSs absorbing in the near infrared region, and specifically in the therapeutic windows in which biological tissues are transparent, is highly suitable. Therefore, different aspects of the PSs should be considered for their optimization: their bioavailability and ideally their ability to localize in tumor cells, their optical properties, and their photophysical evolution, which should allow efficient ISC and the subsequent generation of ROS.

Presently, several PSs have been clinically approved for PDT.[14–16] However, the development of a PS presenting high tumor specificity, low toxicity in the dark, high cytotoxicity upon infrared light activation, sufficient lipophilicity to penetrate the cell membrane, and enhanced solubility in a physiological environment remains challenging.[17] As a rule of thumb, a PS should present a good balance between hydrophilicity and lipophilicity to achieve both physiological solubility and membrane penetration. Temoporfin, also known as mTHPC (*meso*-tetrahydroxyphenylchlorin), is a synthetic tetrapyrrole derivative that contains four phenol groups attached at the *meso* positions to form a chlorin cycle.[18–20] mTHPC has been used as a PDT agent under the commercial name Foscan© since it was approved by the European Medicines Agency (EMA) in 2003. mTHPC is a second-generation photosensitizer, which presents a narrow and intense absorption band at 652 nm falling at the border of the clinical window, undergoes ISC with a high quantum yield, and is stable in biological media.[18,19] However, despite its promising features, the usage of mTHPC within the PDT framework is limited to topical applications or palliative treatments, especially for head and neck cancers, due to its tendency for aggregation, which limits its bioavailability and may alter its photophysical and optical properties. Even though mTHPC has already been approved and commercialized, several strategies are constantly being explored to overcome these shortcomings.[18]

These include the encapsulation of mTHPC with a vectorization agent such as peptides,[21] cyclodextrins (CDs),[22–25] and liposomes[26,27] to increase its solubility, targeting, and tissue penetration abilities. We have shown that the encapsulation of mTHPC can be readily achieved with β-cyclodextrin units in a 2 : 1 ratio,[28] without altering the ISC quantum yields of mTHPC,[24] yet allowing the fast internalization of the drug-delivery complex and its possible spontaneous dissociation in the lipid bilayer core.[23]

Other molecular design strategies are aimed at enhancing the infrared absorption properties of mTHPC to be used in deep tumor treatment. A possible strategy to tackle this issue is to rely on two-photon absorption (TPA) photosensitizers, which in this case may be introduced by suitable functionalization of the tetrapyrrole unit. TPA has been firstly theorized by Maria Göppert-Mayer in 1931 and later observed in the 1960s after the invention of lasers.[29] The mechanism involves the simultaneous absorption of two photons of equal or different energies, going through a virtual state to populate a suitable excited state. If we consider monochromatic light, the electronic transition can, thus, be achieved with photons of half the energy difference between the ground and the excited state; hence, TPA takes place at wavelengths that are doubled compared to single photon absorption. However, since it is a formally forbidden process, TPA probability is usually smaller than single photon absorption. Furthermore, because of the need of simultaneous absorption of two photons, the cross section will depend on the square of the intensity of the light source. Yet, in addition to the displacement of the absorption towards longer wavelengths allowing deeper tissue penetration, TPA offers several advantages to improve PDT efficiency: the TPA cross-section quadratic dependence on the laser intensity increases spatial selectivity since the PDT activation will be restricted to the focal point only minimizing lesions at the border; on the other hand, the low energy of the TPA wavelength minimizes adjacent tissue damage. Yet, such enhancements depend on the development of new photosensitizers characterized by high TPA cross sections (σ) in the near infrared region, since those currently proposed still have low PDT efficiency.

In previous contributions, the TPA cross-section (σ_{TPA}) for mTHPC has been estimated at 28 ± 8 GM at 775 nm in DMSO[30] and 18 GM at 800 nm in 20% ethanol, 30% polyethylene glycol and 50% distilled water.[31] While both experiments suggest the possibility of using mTHPC in TPA-based PDT, the cross section should be higher to allow for efficient light harvesting. For this purpose, Senge *et al.* published a study in 2021 reporting the functionalization of mTHPC with different groups to systematically increase the σ_{TPA} while correlating the increase of the TPA cross section with the PS structure.[32] From the literature, it appears that the increase of σ_{TPA} in tetrapyrrolic systems can be achieved by different strategies. These include, increasing the conjugation length, integration of the ethynyl bridge at β[33] or *meso* positions,[34,35] and functionalization with antennas that already possess a high σ_{TPA}.[36] Herein, we explore the modification of mTHPC with three different TPA-active dyes: DTP1, DTP2, and DPP (Fig. 2) to increase TPA cross sections. To the best of our knowledge, DTP derivatives have not been

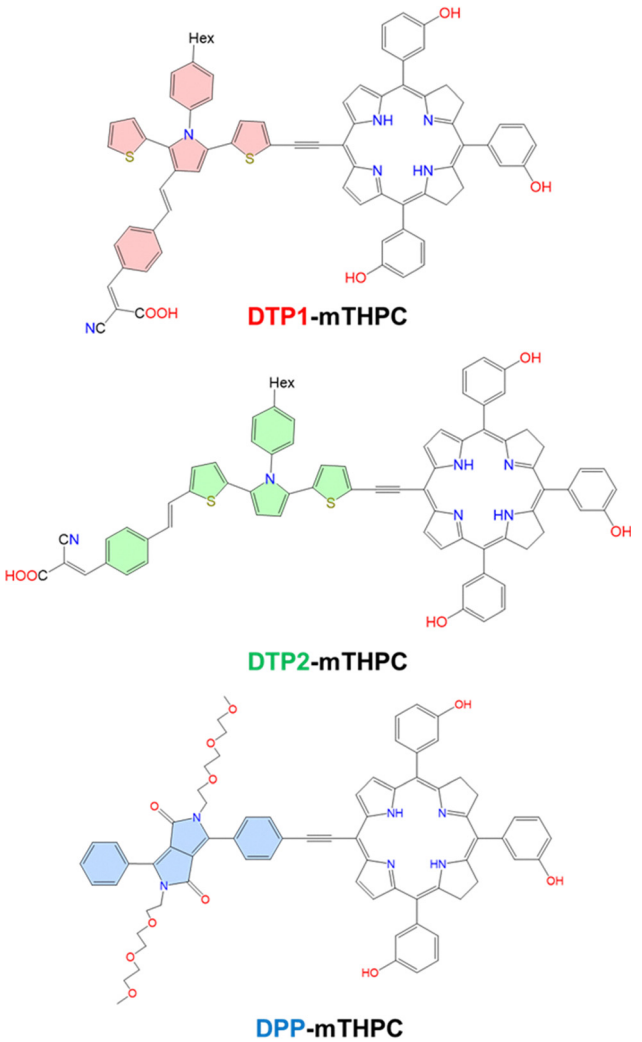

Fig. 2 Structures of proposed TPA-sensitized photosensitizers and TPA antenna moieties are highlighted.

previously incorporated to improve the photophysical properties of tetrapyrrole-derived molecules. DTP are derived from the substitution of a π-chain and an acceptor group to different positions on the 2,5-dithienylpyrrole core,[37–39] and have been extensively analyzed *via* experimental[37] and computational[38,39] methods. DTP1 shows two absorption peaks at 566 nm and 820 nm, whose TPA cross sections are found to be 422.0 and 1243.6 GM, respectively. DTP2, on the other hand, shows σ_{TPA} values of 742 and 6977.7 GM for its peaks at 624 nm and 870 nm, respectively. Moreover, the carboxylic unit on the DTP moiety can be exploited to conjugate small molecules to target specific oncogenic receptors overexpressed in tumor cells.[40,41] Conversely, the TPA cross section of polyethylene glycolated (PEG) diketopyrrolopyrrole (DPP) conjugated with a zinc-bound porphyrin (ZnP) reveals an elevation of the σ_{TPA} at a λ_{max} from 20 GM to 1400 GM.[35] Therefore, the PEGylated DPP molecule has been included in this study, since it provides a suitable comparison to unravel the properties of previously unstudied DTP antennas. However, to our knowledge, this specific temoporfin moiety has not been previously conjugated with PEGylated DPP.

The main objective of this work is to improve the optical properties of mTHPC in order to be used as a PDT agent in the treatment of deep-tissue lesions. To this end, we have designed three novel molecules by combining three high σ_{TPA} compounds (DTP1, DTP2 and DPP) with the original mTHPC molecule (Fig. 2). In line with this purpose, a variety of quantum mechanical (QM) analysis were used to predict the optical and photophysical properties of DTP- and DPP-conjugated mTHPC molecules, such as one-photon absorption (OPA), TPA, spin–orbit coupling (SOC), singlet and triplet energy gaps (Δ_{ST}), and natural transition orbitals (NTOs). Subsequently, benefiting from molecular dynamics (MD) simulations, PSs were simulated in various environments that mimic biological conditions, such as bulk water and in interaction with a lipid bilayer mimicking a cellular membrane. Furthermore, to address the solubility issue, the candidate PSs were encapsulated with β-CDs. Two CD units have been used to encapsulate DTP1-mTHPC and DTP2-mTHPC, while in the case of DPP-mTHPC only one CD was used since the presence of the polyethylene glycol (PEG) groups induce potential steric clashes and already improved the overall solubility. Randomly selected snapshots from classical MD simulations have also been extracted to calculate vertical absorption energies and cross sections at the QM/MM level to observe if the absorption patterns were influenced by these environmental parameters.

Computational methodology

Quantum mechanical calculations

All geometry optimizations and single-point excited state calculations were performed with the Gaussian 16 program package.[42] The ground and excited state geometry optimizations were done both *in vacuo* and in water solution modeled with the polarizable continuum method (PCM).[43,44] Ground state geometry optimizations were performed at the density functional theory (DFT) level using the meta-hybrid M06-2X[45] functional as its performance was shown to be superior in describing the ground state of chlorin type molecules compared to the B3LYP functional.[24,46] Though the 6-31+G(d) basis set was shown to be sufficient to describe the electronic properties of mTHPC in a previous study,[24] to better account for the changes rising from the inclusion of the TPA antenna the 6-31+G(d,p) basis set was employed for all QM calculations. On top of the optimized ground state geometry, the performance of different functionals in reproducing the vertical excitation energies using time dependent-DFT (TD-DFT) was assessed. The selected exchange–correlation functionals included CAM-B3LYP,[47] LC-BLYP[48] and ωB97XD[49] *in vacuo* and water and the results are reported in ESI,† Fig. S1. To better compare with the experimental spectra all the vertical transitions were convoluted using Gaussian functions of a full-width at half length (FWHL) of 0.2 eV.

Furthermore, to obtain more realistic absorption properties, sampling of the Wigner distribution around the S_0 and S_1 minima geometry based on the vibrational degrees of freedom

and vibrational frequencies was performed *via* the NewtonX program.[50] From 100 initial geometries, 40 structures were selected to perform TD-DFT calculations using the aforementioned three functionals for the first 20 excited singlet states. Based on these results, we selected the ωB97XD functional with the 6-31+G(d,p) basis set for further modeling and geometry optimization of the relevant excited states. This also aligns with the fact that the ωB97XD functional has been shown to accurately describe the experimental vertical transitions of mTHPC and DTP derivatives.[24,51] To calculate the TPA cross sections of the antenna-mTHPC systems, the publicly available Dalton2020 program package[52] was used. The linear response methodology calculations were executed *in vacuo* at the CAM-B3LYP/6-31G(d) level of theory. In previous benchmarks from different studies, comparing different DFT functionals available in the Dalton package, CAM-B3LYP was found to outperform other functionals for TPA calculations.[53,54] The Nancy_EX code[55–57] was used to obtain the natural transition orbitals (NTOs) and the topological Φ_s indices, characterizing the electronic excited state's nature in terms of the electronic density rearrangement. NTOs were visualized with the Avogadro visualization and analysis program.[58] Additionally, the Amsterdam Modeling Suite AMS/2022.103 package[59] was used for the singlet–triplet split and SOC calculations at the DFT level with the ωB97XD functional using 40 initial geometries sampled by Wigner distribution around the S_0 and S_1 minima, respectively. The DZP basis set together with ZORA scalar and TD-DFT methods was employed within a water environment, which was modeled with the integral equation formalism polarizable continuum model (IEF-PCM). As AMS does not support Pople type basis sets, DZP basis was chosen as a good compromise between accuracy and computational costs.

Molecular dynamics simulations and QM/MM

The Amber22 program package[60,61] was used to perform classical MD calculations. Force field parameters for each candidate PS were attained using the Antechamber package[62] in conjunction with the Generalized Amber Force Field 2 (GAFF2).[63] The structures of the CD units were obtained from the protein data bank (PDB ID:3CGT[64]) consistent with a previous study[65] and modeled using the GLYCAM06_j[66] force field. The lipid bilayer used to model the biological membrane was built using the CHARMM-GUI[67] web-server and consists of 150 1-palmitoyl-2-oleoyl-*sn-glycero*-3-phosphocholine (POPC) units on each layer hydrated with 14 808 TIP3P[68] water molecules. Counterions (K^+ and Cl^-) are used to ensure a neutral simulation box and a physiological (0.15 M) salt concentration. POPC was chosen as the model lipid to allow a direct comparison with our previous work,[23,24] and due to its ability to reproduce the behavior of eukaryotic cellular membranes, the Amber Lipid17 Force Field[69] was used to represent the bilayer. It's worth noting that in a previous study where we modeled mTHPC in similar environments, these computational conditions have proven capable of reproducing the experimental behavior.[24] Note that, while the use of a POPC-only lipid bilayer is a commonly used model for membrane interactions, because of the absence of asymmetry and other components such as other lipid types and cholesterol to make it realistic, the model could have some limitations to elucidate the photosensitizer's behavior in a physiological environment.

Simulations were propagated in the constant pressure and temperature (NPT) ensemble at 1 atm and 300 K. Temperature control relied on the Langevin thermostat,[70] while pressure regulation used the Berendsen barostat.[71] Long-range electrostatic interactions were calculated through the particle-mesh-Ewald method,[72] employing an 8 Å cutoff distance, while periodic boundary conditions (PBCs) were consistently used. For each simulation, hydrogen mass repartition (HMR)[73] was used in combination with the Rattle and Shake algorithms[74] to slow the highest frequency vibrations involving hydrogens, thus allowing the use of a 4.0 fs time step to integrate Newton's equations of motion.

As aforementioned, three distinct environments were explored: the aqueous phase, β-CD encapsulation, and interaction with a lipid bilayer. Equilibration involved gradual heating over 10 ps from 0 to 300 K. Membrane equilibration utilized a protocol for gradual restraint removal to ensure stability, therefore, the constraints on the heavy atoms of the POPC were progressively reduced in three consecutive steps of 36 ns each. The production simulations lasted 500 ns for each environment.

MD trajectories were analyzed with CPPTRAJ[75] of AmberTools23[76] and VMD,[77] the membrane thickness, area per lipid, and density profiles were obtained using the MEMBPLUGIN[78] extension and Density Profile Tool,[79] respectively.

For the QM/MM study of the absorption spectra, the Terachem/Amber[80] interface was used to obtain the absorption spectra of the PS in different simulated environments. Using the CPPTRAJ tool, 100 snapshots from each simulation except *in vacuo* have been extracted. On top of these snapshots, vertical transitions have been calculated at the TD-DFT level with the ωB97XD/6-31+G(d,p) protocol. The whole PS molecule (TPA-mTHPC) was included in the quantum partition, whereas water, β-CD and POPC lipids were treated at the MM level.

Results and discussion

Optical properties

The simulated OPA and TPA absorption spectra of the three antenna-sensitized chromophores are reported in Fig. 3, together with the most relevant NTOs describing the lowest state with the highest cross sections for OPA and TPA, respectively. As expected, the shape of the OPA spectra resembles one of a porphyrin-like systems, notably characterized by the presence of the Q- and Soret-bands in the visible and infrared regions, respectively. Notably, the position of the Q-band is only slightly altered by the presence of the antenna. In addition, and mostly in the visible range, additional bands that may be assigned to absorption centered on the antennas are also present. Intermolecular charge-transfer states featuring transitions between the two moieties are safely excluded, at least in

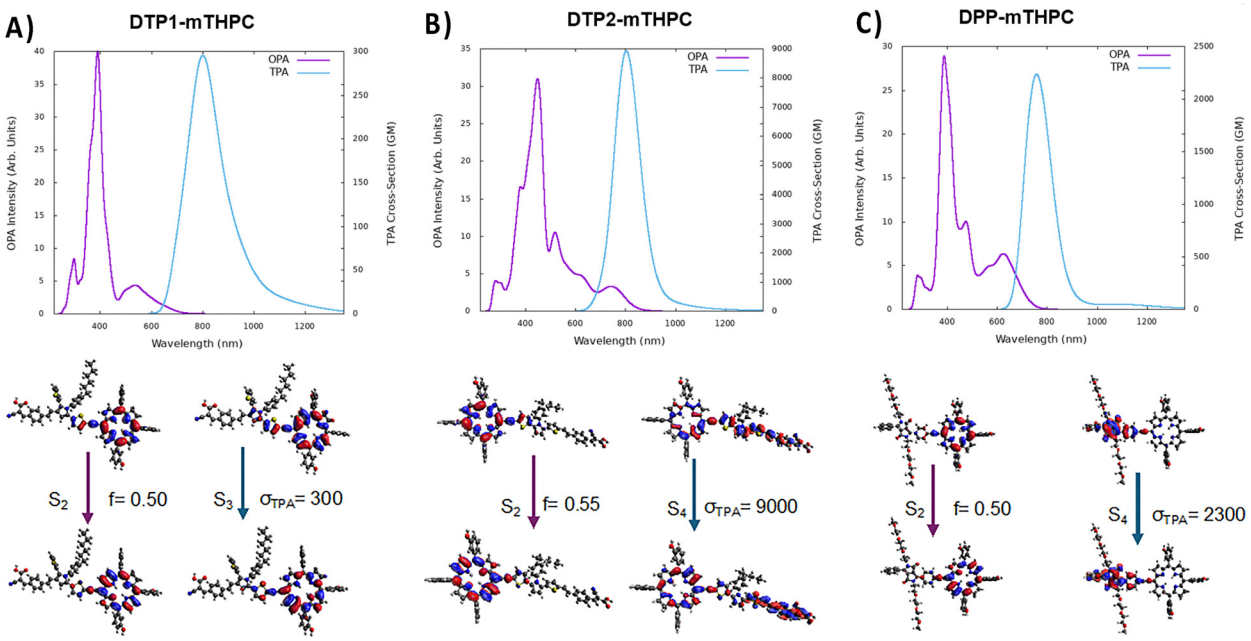

Fig. 3 Normalized one-photon (ωB97XD/6-31+G(d,p)) and two-photon (CAM-B3LYP/6-31G(d)) absorption spectra of (A) DTP1-mTHPC, (B) DTP2-mTHPC and (C) DPP-mTHPC molecules, together with their corresponding λ_{max} (eV) and σ (GM) values. The NTOs belonging to the most probable transitions were also reported.

the low energy portion of the spectrum. However, especially in the case of the DTP2-sensitized compound, delocalized excitations spanning the whole molecular systems can be observed, notably for S_4. The fluorescence absorption (Fig. S6, ESI†) was also modeled showing that for each molecule the emission takes place from a porphyrin-centered state, and thus is only marginally sensitive to the presence of the antenna. However, if the modification of the one-photon optical properties brought by the antenna are only marginal, more subtle and significant changes can be accessed in the TPA spectra. Indeed, it was reported that the functionalization of the parent chromophore, such as through the addition of carbonyl groups, alkyne linkers and high two-photon absorbing molecules have a significant effect in increasing the TPA cross section.[81–86]

All three antenna-sensitized molecules show a relevant and rather intense TPA capacity in the infrared region (Fig. 3); however, significant differences should be pointed out. Indeed, mTHPC-DTP1 presents a large and rather asymmetric band. Interestingly, the most intense TPA excitation involves the porphyrin Q-band S_3 state peaking at 300 GM. The asymmetry of the band is instead due to the TPA excitation of the DTP1 moiety, which has a lower inherent cross section, as already shown in our previous work.[38] Therefore, the functionalization with DTP1 appears suboptimal for the purpose of increasing the TPA capacity of the PS. This situation is instead reverted in the case of mTHPC-DPP, which presents a high cross section at around 800 nm exceeding 2250 GM.

Interestingly, as shown by the corresponding NTOs, this transition is due to a DPP-based excited state, which is inherently TPA-active. However, the most striking TPA potential is observed for mTHPC-DTP2, which presents an impressive infrared cross section achieving 9000 GM. This value largely outperforms the performance observed for the parent DTP2, which already presented the best TPA cross section among its series. The enhancement of TPA activity upon conjugation with the porphyrin core may be rationalized by the presence of strongly delocalized excitation (S_4), which extends over the whole molecular system. This result is also extremely promising for potential applications, since mTHP-DTP2 presents strong TPA in a spectral region compatible with the therapeutic window, thus allowing the treatment of deeper lesions.

Photophysics and intersystem crossing efficiency

The presence of a facile intersystem crossing (ISC) presenting a high quantum yield is fundamental to allow the population of the triplet state and, consequently, the energy transfer to the ground state $^3O_2$ leading to the activation of the cytotoxic $^1O_2$. To analyze the suitability of the ISC relaxation channel, we have obtained the energy level diagram of the singlet and triplet states at Franck–Condon (SI) and at the S_1 optimized geometry (Fig. 4). Indeed, a region of singlet–triplet quasi-degeneration is needed to allow the non-adiabatic ISC process. Furthermore, since an ultrafast relaxation *via* the fully spin-allowed internal conversion (IC) is expected from the S_1 equilibrium which represents the most crucial region.

In Fig. 4 we report the average energy value of the singlet and triplet states obtained from a Wigner sampling of the S_1 minimum. The standard deviation is also provided to highlight the spread of the energy distribution upon vibrational movement. We immediately observe that mTHPC-DTP1 and mTHPC-DTP2 present nearly ideal conditions to assure ISC (Tables S2 and S3 for DTP1-mTHPC and Tables S4 and S5 for DTP2-

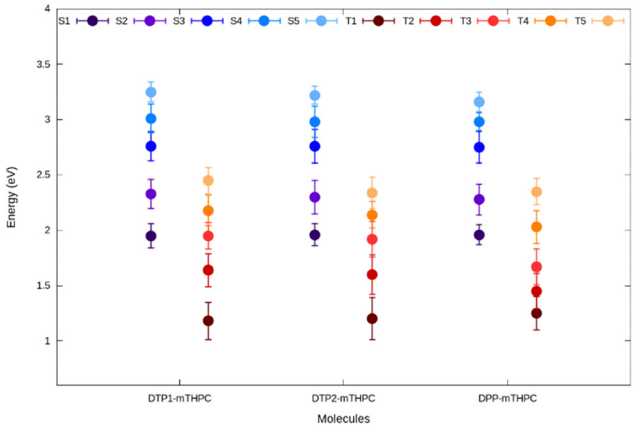

Fig. 4 Average value (standard deviation included) of the singlet and triplet energies obtained by sampling the S_1 minimum *via* a Wigner distribution.

mTHPC, ESI†). Indeed a (quasi)-degeneracy between the energies of the S_1 and the T_3 states exist for both systems, the maximum gap observed for mTHPC-DTP2 being of only 0.038 eV (Tables S4 and S5, ESI†). Therefore, we propose that both systems will follow a photophysical pathway involving the $S_1 \rightarrow T_3$ ISC followed by fast IC in the triplet manifold to reach T_1. While this pathway is probable, given the energy degeneracy, it should be pointed out that SOC elements between S_1 and T_3 are weak amounting at 0.136 and 0.142 cm^{-1} for mTHPC-DTP1 (Tables S8 and S9, ESI†) and mTHPC-DTP2 (Tables S10 and S11, ESI†), respectively. It is worth noting that according to the El-Sayed rules, as the nature of the molecular orbitals involved in these transitions are all π–π*, the computed SOCs are rather small, although SOC values between 0.2 and 5.0 cm^{-1} are considered large enough to induce ISC on a nanosecond time scale. Considering the closest singlet–triplet energy states of parent mTHPC, the SOC value belonging to that transition ($S_1 \rightarrow T_4$) is found to be 0.2 cm^{-1}.[87] Even if the low value of the SOC can significantly slow ISC, similar coupling elements were observed for the parent mTHPC, which is known to activate singlet oxygen, confirming the suitability of the proposed approach.

Conversely, mTHPC-DPP stands apart showing larger differences in the distribution of the excited states. Indeed, for this molecule the T_4 average energy level lies 0.068 eV higher than S_1, while T_3 is closed in energy about 0.25 eV from the first singlet excited state (Tables S6 and S7, ESI†). However, since the distribution of the energy levels of T_4 and S_1 sampled by a Wigner distribution are still largely overlapping (Fig. 4), we may assume that ISC will proceed through the non-adiabatic transition to T_4, probably characterized by a lower quantum yield compared to the other chromophores, followed once again by the fast IC to reach the population of T_1. As it was the case for the other compounds, the SOC elements between the two most plausible states are weak (0.267 cm^{-1}) (Tables S12 and S13, ESI†), further pointing to the non-ultrafast and non-unitary quantum yield of the process.

Interaction of the PSs with the lipid bilayer and passive drug delivery

Having confirmed that the proposed PS candidates may be regarded as efficient TPA sensitizers, which can potentially undergo ISC and, hence, activate singlet oxygen, we decided to study their interaction with a model lipid bilayer, which represents an ideal target for the PDT approach. In a previous study,[24] we have already shown that the parent mTHPC is internalized in the lipid bilayer residing in proximity to the polar heads, its density distribution partially overlapping with the position of the lipid tail double-bond, which is a target of oxidation by $^1O_2$. By using classical MD simulations, we have shown (Fig. 5) that all candidate PS molecules interact persistently with the lipid bilayer and in particular position themselves in the polar head-region. The interaction between the PS and the membrane takes place spontaneously and is persistent along the time-scale of the MD simulation, suggesting the formation of a stable complex (Fig. S9 and S10, ESI†). Consistent with the behavior of the parent porphyrin moiety,[24] we observe a partial overlap of the density distribution of the PS with that of the lipid tail, indicating a favorable positioning to allow $^1O_2$ activation in proximity to its biological target. Interestingly, mTHPC-DPP seems to penetrate deeper into the membrane hydrophobic core, as shown by its density profile. However, this fact is mostly due to the PEG tails rather than the porphyrin core, which remains strongly anchored to the polar head region. The porphyrin ring interacts with the polar head through cation–π interactions, specifically between the quadrupole of the phenol ring attached to the porphyrin and positively charged quarter amine moiety of the lipid polar head.

As shown in the ESI† (Fig. S11–S13), the chromophore is maintained at the polar head interface by a subtle combination and balance of different interactions involving notably the dispersion between the lipid tails and the hydrophobic core of the chromophore. In addition, cation–π and alkyl–π interactions are formed with the phosphatidyl choline, palmitoyl acyl and monounsaturated oleoyl acyl moieties (Tables S15–S17, ESI†). Interestingly, in the case of mTHPC-DPP only the porphyrin core leaving the antenna free to bury into the lipid bilayer.

Interestingly, mTHPC part of the molecule, is also the only compound showing the emergence of hydrogen bonds albeit quite labile.

One of the main drawbacks suffered by PDT drugs is their limited bioavailability, due to the presence of hydrophobic extended conjugated moieties leading to poor water solubility. To overcome this issue, passive drug delivery strategies can be envisaged consisting of encapsulating the drug with a water-soluble hollow carrier, such as cyclodextrin (CD)[28] or calixarenes.[88] In previous studies,[23,24] we have shown that mTPHC encapsulation by β-CD is an efficient strategy increasing water solubility without preventing the internalization into the lipid membrane. Thus, we explore this possibility with our proposed PSs anchored with TPA antenna. As seen in Fig. 6 and Fig. S14 (ESI†), the DTP1- and DTP2-functionalized chromophores form a 1:2 complex with β-CD, similar to the behavior of the parent mTHPC.[24,28] Notably while the β-CD encapsulates the porphyrin core, the TPA antenna remains largely exposed to the solvent. This fact can, however, facilitate its inclusion in the lipid bilayer enhancing the amphiphilicity of the drug. Both DTP1 and DTP2 give rise to stable and

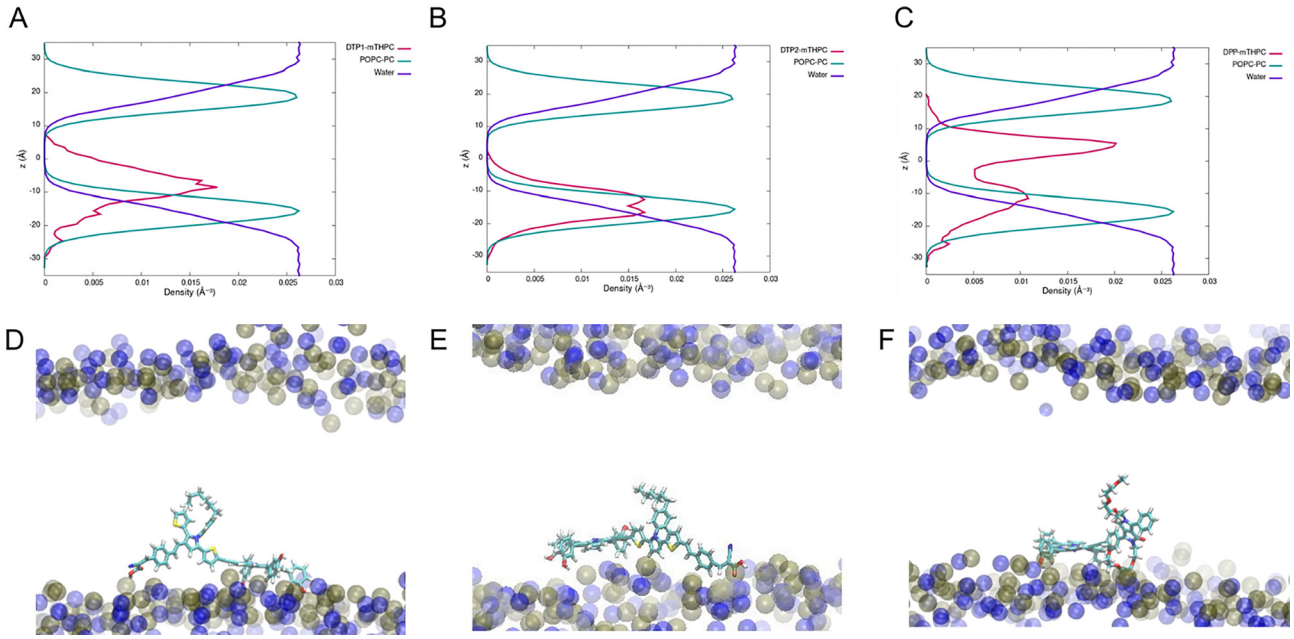

Fig. 5 Density distribution profile along the membrane axis for the chromophore, the lipid tails, and water for mTHPC-DTP1 (A), mTHPC-DTP2 (B), and mTHPC-DPP (C). Representative snapshots at the equilibrium position are shown for mTHPC-DTP1 (D), mTHPC-DTP2 (E), and mTHPC-DPP (F).

persistent complexes and the distance between the center of mass of mTHPC and the β-CD remains stable with a distribution peaked at around 8 Å (Fig. 6). Interestingly, DTP2 seems to form a slightly more loosely bound complex presenting a larger distance between the center of mass at about 9 Å. In the case of mTHPC-DPP we only attempted to build a 1 : 1 complex with the CD, due to the larger steric hindrance of the PEG moieties, and their increased hydrophilic character. However, the complex with the CD is highly persistent even if the maximum value of the distance between the center of mass increases up to 11 Å. Similar to what was observed for the parent mTHPC, the encapsulation reduces the rotational movements of the phenyl substituents, while the flexibility of the solvent exposed antenna is not altered (Fig. S15, ESI†).

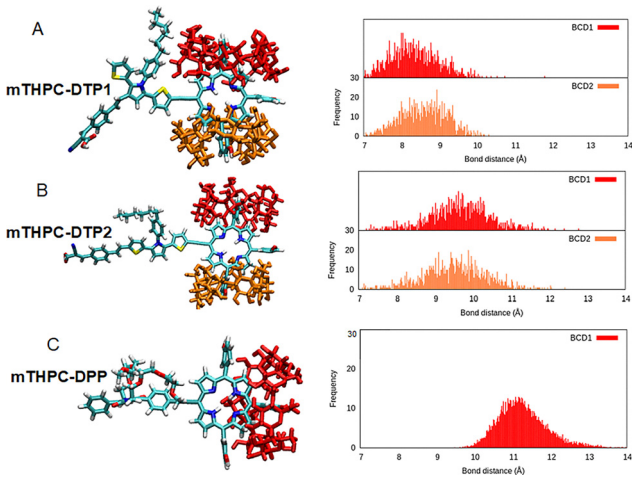

Fig. 6 Representative snapshots of the complex between the PS and CD, the distribution of the distance between the center of mass of mTHPC and the complexing CD is also reported. (A) mTHPC-DTP1, (B) mTHPC-DTP2, and (C) mTHPC-DPP.

Finally, to assess the influence of the encapsulation and membrane interaction on the optical properties of our chromophores we calculated the OPA spectrum by extracting snapshots from MD with the chromophore placed either in water, inside a lipid bilayer, or encapsulated with CD (Fig. 7). Besides some minor differences, results confirm that the main features of the spectra, as described in the previous section, are largely unchanged. More importantly, no significant modification in the position or the shape of the main absorption bands is observed between the different environments. This result is highly encouraging since it suggests that the photophysical pathway leading favorably to $^1O_2$ activation should hold under different conditions potentially experienced by the PDT agent. However, a further study involving the photophysical pathways of TPA-decorated mTHPC in different explicit environments should be performed, ideally with non-adiabatic QM/MM dynamics to confirm this assumption.

Conclusions

By resorting to a multiscale approach involving ground and excited state quantum chemistry simulations as well as classical MD and QM/MM simulations, we proposed an original strategy to enhance the PDT efficiency of the mTHPC drug. In particular, we show that the functionalization of mTHPC with different TPA antennae is suitable to significantly increase the TPA cross section leading to an intense absorption band in the infrared region. In particular, the functionalization with DTP2 leads to an impressive TPA cross section σ_{TPA} of about 9000 GM, rarely observed for organic chromophores. Furthermore,

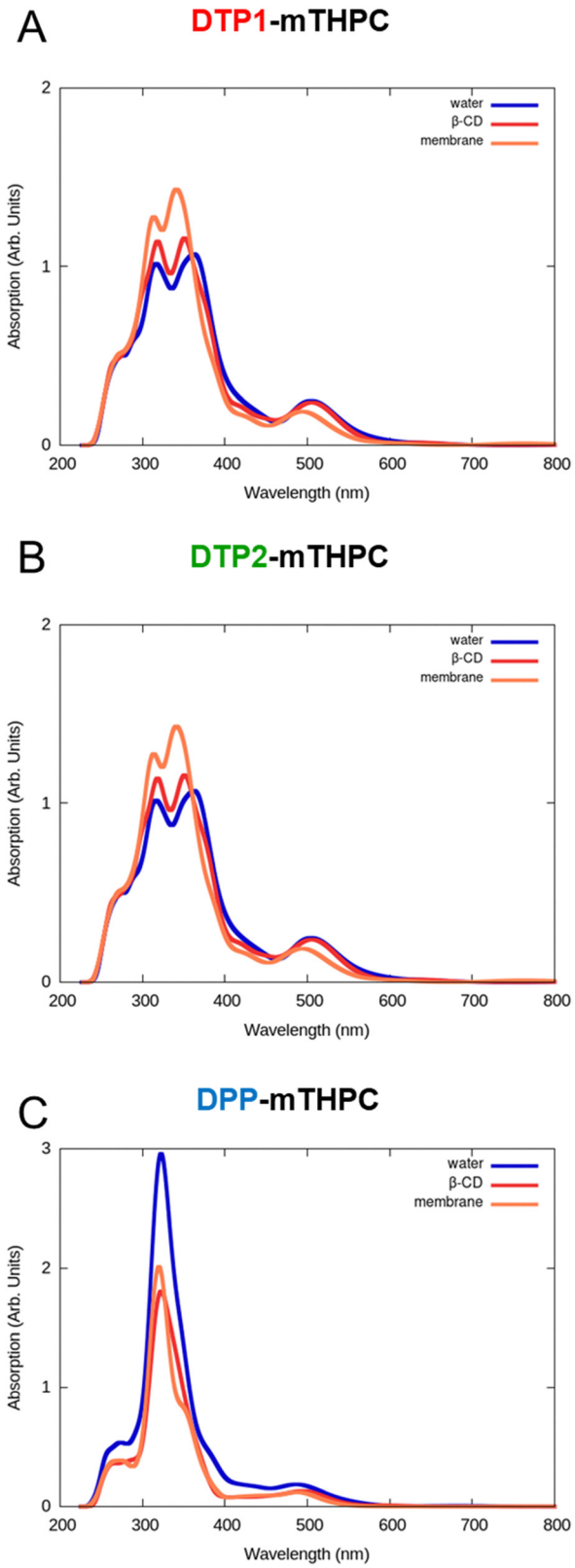

Fig. 7 Calculated (at ωB97XD/6-31+G(d,p)) normalized absorption spectrum of TPA-anchored mTHPC molecules in different environments: in water (blue), 2PA-mTHPC:β-CD in water (red) and in proximity of the lipid membrane (orange) for DTP1-mTHPC (A), DTP2-mTHPC (B) and DPP-mTHPC (C). The ground state conformational space has been sampled with 500 ns equilibrium MD.

we have also shown that the TPA functionalization preserves the favorable photophysical routes leading to ISC, and thus $^1O_2$ activation. Indeed, especially in the case of DTP1- and DTP2-functionalized PSs an almost perfect degeneracy between T_3 and S_1 holds at the S_1 equilibrium geometry. Such alignment of states should provide efficient ISC, despite the small values of the SOC. On the contrary, ISC for mTHPC-DPP should be slightly less efficient and be allowed by vibrational activation.

Finally, we have confirmed that all TPA-functionalized compounds may be readily internalized in lipid bilayers, persistently residing at the polar head and presenting some overlap with the position of the lipid tail double bonds, which are the primary target of the activated singlet oxygen. In addition, we have also confirmed that the TPA-sensitized PS could potentially be encapsulated with CD moieties for passive delivery, consistent with the strategy used for the parent mTHPC drug.[23,24,28] Importantly, the different molecular environments do not alter the optical properties of the drug candidates, suggesting the robustness of the ISC pathways.

Our computational approach has allowed the proposition of TPA-sensitized PSs, which present extremely high TPA cross sections combined with a facile ISC and membrane internalization capabilities. As such they may represent a most promising solution for the PDT treatment of deeper lesions exploiting IR excitation. In the future, we plan to study the interaction of the encapsulated PS with the model lipid bilayer to confirm the efficient delivery of the drug. Furthermore, the photophysical pathway leading to ISC upon excitation of the TPA-active singlet state will be explored by surface-hopping non-adiabatic dynamics simulations, eventually at the QM/MM level. Yet, we believe that our study already highlights the power of computational chemistry and rational molecular design in proposing novel PDT agents, paving the way for future experimental validation and clinical translation.

Author contributions

A. M. and S. C. conceived the project and computational simulation strategy. B. K. F. and E. S. U. carried out the calculations and characterization. B. K. F., A. M. and S. C. discussed the results and thoroughly revised the manuscript. All authors interpreted the data and contributed to the preparation of the manuscript.

Conflicts of interest

There are no conflicts to declare.

Data availability

Data for this article, including all necessary files for generating the initial structures of two-photon antenna-conjugated Temoporfin (mTHPC) in various environments, are publicly available on GitHub at **https://github.com/basakkf/2PA-mTHPC**.

Acknowledgements

The authors thank GENCI, Explor and the National Center for High Performance Computing of Turkey (UHeM) under grant number 1011062021, computing centers and the Platform P3MB for computational resources. The authors thank ANR and CGI for their financial support of this work through Labex SEAM ANR 11 LABEX 086, ANR 11 IDEX 05 02 and PIRATE, and the support of the IdEx ''Université Paris 2019'' ANR-18-IDEX-0001. Support from the PEPR LUMA is also gratefully acknowledged. B. K. F., E. S. U. and S. C. thank TUBITAK (Project Number 120Z659) for financial support. B. K. F. would also like to thank the French Embassy in Turkey for a joint PhD grant.

References

1 P. Agostinis, K. Berg, K. A. Cengel, T. H. Foster, A. W. Girotti, S. O. Gollnick, S. M. Hahn, M. R. Hamblin, A. Juzeniene, D. Kessel, M. Korbelik, J. Moan, P. Mroz, D. Nowis, J. Piette, B. C. Wilson and J. Golab, Photodynamic therapy of cancer: An update, *Ca-Cancer J. Clin.*, 2011, **61**, 250–281.

2 J. H. Correia, J. A. Rodrigues, S. Pimenta, T. Dong and Z. Yang, Photodynamic Therapy Review: Principles, Photosensitizers, Applications, and Future Directions, *Pharmaceutics*, 2021, **13**, 1332.

3 M. Penetra, L. G. Arnaut and L. C. Gomes-da-Silva, Trial watch: an update of clinical advances in photodynamic therapy and its immunoadjuvant properties for cancer treatment, *OncoImmunology*, 2023, **12**, 2226535.

4 C. A. Robertson, D. H. Evans and H. Abrahamse, Photodynamic therapy (PDT): A short review on cellular mechanisms and cancer research applications for PDT, *J. Photochem. Photobiol., B*, 2009, **96**, 1–8.

5 M. C. DeRosa and R. J. Crutchley, Photosensitized singlet oxygen and its applications, *Coord. Chem. Rev.*, 2002, **233–234**, 351–371.

6 M. S. Baptista, J. Cadet, P. Di Mascio, A. A. Ghogare, A. Greer, M. R. Hamblin, C. Lorente, S. C. Nunez, M. S. Ribeiro, A. H. Thomas, M. Vignoni and T. M. Yoshimura, Type I and Type II Photosensitized Oxidation Reactions: Guidelines and Mechanistic Pathways, *Photochem. Photobiol.*, 2017, **93**, 912–919.

7 L. K. McKenzie, H. E. Bryant and J. A. Weinstein, Transition metal complexes as photosensitisers in one- and two-photon photodynamic therapy, *Coord. Chem. Rev.*, 2019, **379**, 2–29.

8 A.-G. Niculescu and A. M. Grumezescu, Photodynamic Therapy—An Up-to-Date Review, *Appl. Sci.*, 2021, **11**, 3626.

9 S. Kwiatkowski, B. Knap, D. Przystupski, J. Saczko, E. Kędzierska, K. Knap-Czop, J. Kotlińska, O. Michel, K. Kotowski and J. Kulbacka, Photodynamic therapy – mechanisms, photosensitizers and combinations, *Biomed. Pharmacother.*, 2018, **106**, 1098–1107.

10 U. Chilakamarthi and L. Giribabu, Photodynamic Therapy: Past, Present and Future, *Chem. Rec.*, 2017, **17**, 775–802.

11 B. Koca-Findik, E. Lognon, S. Catak and A. Monari, In Silico Study of Active Delivery of a Photodynamic Therapy Drug Targeting the Folate Receptor, *Photochem. Photobiol. Sci.*, 2025, 9, DOI: 10.1007/s43630-025-00745-4.

12 M. Baydoun, L. Boidin, B. Leroux, A.-S. Vignion-Dewalle, A. Quilbe, G. P. Grolez, H. Azaïs, C. Frochot, O. Moralès and N. Delhem, Folate Receptor Targeted Photodynamic Therapy: A Novel Way to Stimulate Anti-Tumor Immune Response in Intraperitoneal Ovarian Cancer, *Int. J. Mol. Sci.*, 2023, **24**, 11288.

13 M. Baydoun, O. Moralès, C. Frochot, C. Ludovic, B. Leroux, E. Thecua, L. Ziane, A. Grabarz, A. Kumar, C. De Schutter, P. Collinet, H. Azais, S. Mordon and N. Delhem, Photodynamic Therapy Using a New Folate Receptor-Targeted Photosensitizer on Peritoneal Ovarian Cancer Cells Induces the Release of Extracellular Vesicles with Immunoactivating Properties, *J. Clin. Med.*, 2020, **9**, 1185.

14 R. R. Allison and C. H. Sibata, Oncologic photodynamic therapy photosensitizers: A clinical review, *Photodiagn. Photodyn. Ther.*, 2010, **7**, 61–75.

15 R. R. Allison, G. H. Downie, R. Cuenca, X. H. Hu, C. J. H. Childs and C. H. Sibata, Photosensitizers in clinical PDT, *Photodiagn. Photodyn. Ther.*, 2004, **1**, 27–42.

16 M. R. Detty, S. L. Gibson and S. J. Wagner, Current clinical and preclinical photosensitizers for use in photodynamic therapy, *J. Med. Chem.*, 2004, **47**, 3897–3915.

17 H. Abrahamse and M. R. Hamblin, New photosensitizers for photodynamic therapy, *Biochem. J.*, 2016, **473**, 347–364.

18 A. Wiehe and M. O. Senge, The Photosensitizer Temoporfin (mTHPC) – Chemical, Pre-clinical and Clinical Developments in the Last Decade, *Photochem. Photobiol.*, 2023, **99**, 356–419.

19 M. O. Senge and J. C. Brandt, Temoporfin (Foscan®, 5,10,15,20-Tetra(m-hydroxyphenyl)chlorin)—A Second-generation Photosensitizer, *Photochem. Photobiol.*, 2011, **87**, 1240–1296.

20 D. Wöhrle, A. Hirth, T. Bogdahn-Rai, G. Schnurpfeil and M. Shopova, Photodynamic therapy of cancer: Second and third generations of photosensitizers, *Russ. Chem. Bull.*, 1998, **47**, 807–816.

21 Y. Cheng, Q. Chen, Z. Qian, T. Shan, L. Bai, X. Jiang, C. Li, Y. Wang, Y. Cheng, Q. Chen, Z. Qian, T. Shan, L. Bai, X. Jiang, Y. Wang and C. Li, Versatile Red Blood Cells for Triple-Negative Breast Cancer Treatment via Stepwise Photoactivations, *Adv. Healthcare Mater.*, 2023, **12**, 2201690.

22 I. Yakavets, S. Gräfe, L. Bezdetnaya, V. Zorin, H.-P. Lassalle, E. Bastien, I. Khludeyev and I. Yankovsky, Inclusion complexation with β-cyclodextrin derivatives alters photodynamic activity and biodistribution of meta-tetra(hydroxyphenyl)chlorin, *Eur. J. Pharm. Sci.*, 2016, **91**, 172–182.

23 B. Koca Fındık, I. Yakavets, H.-P. Lassalle, S. Catak and A. Monari, Efficient Delivering of a Photodynamic Therapy Drug into Cellular Membranes Rationalized by Molecular Dynamics, *J. Phys. Chem. B*, 2024, **128**, 11625–11633.

24 B. Aslanoglu, I. Yakavets, V. Zorin, H. P. Lassalle, F. Ingrosso, A. Monari and S. Catak, Optical properties of

photodynamic therapy drugs in different environments: The paradigmatic case of temoporfin, *Phys. Chem. Chem. Phys.*, 2020, **22**, 16956–16964.

25 I. Yakavets, M. Millard, V. Zorin, H. P. Lassalle and L. Bezdetnaya, Current state of the nanoscale delivery systems for temoporfin-based photodynamic therapy: Advanced delivery strategies, *J. Controlled Release*, 2019, **304**, 268–287.

26 I. Yakavets, M. Millard, L. Lamy, A. Francois, D. Scheglmann, A. Wiehe, H. P. Lassalle, V. Zorin and L. Bezdetnaya, Matryoshka-Type Liposomes Offer the Improved Delivery of Temoporfin to Tumor Spheroids, *Cancers*, 2019, **11**(9), 1366.

27 M. J. Bovis, J. H. Woodhams, M. Loizidou, D. Scheglmann, S. G. Bown and A. J. MacRobert, Improved in vivo delivery of m-THPC via pegylated liposomes for use in photodynamic therapy, *J. Controlled Release*, 2012, **157**, 196–205.

28 I. Yakavets, H. P. Lassalle, I. Yankovsky, F. Ingrosso, A. Monari, L. Bezdetnaya and V. Zorin, Evaluation of temoporfin affinity to β-cyclodextrins assuming self-aggregation, *J. Photochem. Photobiol., A*, 2018, **367**, 13–21.

29 P. Cronstrand, Y. Luo and H. Ågren, Multi-Photon Absorption of Molecules, *Adv. Quantum Chem.*, 2005, **50**, 1–21.

30 X. Li, B. De Zheng, X. H. Peng, S. Z. Li, J. W. Ying, Y. Zhao, J. D. Huang and J. Yoon, Phthalocyanines as medicinal photosensitizers: Developments in the last five years, *Coord. Chem. Rev.*, 2019, **379**, 147–160.

31 M. Atif, P. E. Dyer, T. A. Paget, H. V. Snelling and M. R. Stringer, Two-photon excitation studies of m-THPC photosensitizer and photodynamic activity in an epithelial cell line, *Photodiagn. Photodyn. Ther.*, 2007, **4**, 106–111.

32 P. Gierlich, S. G. Mucha, E. Robbins, L. C. Gomes-da-Silva, K. Matczyszyn and M. O. Senge, One-photon and two-photon photophysical properties of tetrafunctionalized Temoporfin (m-THPC) derivatives as potential agents for two-photon induced photodynamic therapy, *ChemPhotoChem*, 2022, **6**, e202100249.

33 J. Zhang, K.-L. Wong, W.-K. Wong, N.-K. Mak, D. W. J. Kwong and H.-L. Tam, Two-photon induced luminescence, singlet oxygen generation, cellular uptake and photocytotoxic properties of amphiphilic Ru(II) polypyridyl–porphyrin conjugates as potential bifunctional photodynamic therapeutic agents, *Org. Biomol. Chem.*, 2011, **9**, 6004–6010.

34 T. Zhang, R. Lan, L. Gong, B. Wu, Y. Wang, D. W. J. Kwong, W.-K. Wong, K.-L. Wong and D. Xing, An Amphiphilic BODIPY-Porphyrin Conjugate: Intense Two-Photon Absorption and Rapid Cellular Uptake for Two-Photon-Induced Imaging and Photodynamic Therapy, *ChemBioChem*, 2015, **16**, 2357–2364.

35 J. Schmitt, V. Heitz, A. Sour, F. Bolze, H. Ftouni, J. F. Nicoud, L. Flamigni and B. Ventura, Diketopyrrolopyrrole-porphyrin conjugates with high two-photon absorption and singlet oxygen generation for two-photon photodynamic therapy, *Angew. Chem., Int. Ed.*, 2015, **54**, 169–173.

36 K. Ogawa and Y. Kobuke, Design of two-photon absorbing materials for molecular optical memory and photodynamic therapy, *Org. Biomol. Chem.*, 2009, **7**, 2241–2246.

37 W. Sharmoukh, A. Attanzio, E. Busatto, T. Etienne, S. Carli, A. Monari, X. Assfeld, M. Beley, S. Caramori and P. C. Gros, 2,5-Dithienylpyrrole (DTP) as a donor component in DTP-π-A organic sensitizers: Photophysical and photovoltaic properties, *RSC Adv.*, 2015, **5**, 4041–4050.

38 O. Sengul, M. Marazzi, A. Monari and S. Catak, Photophysical Properties of Novel Two-Photon Absorbing Dyes: Assessing Their Possible Use for Singlet Oxygen Generation, *J. Phys. Chem. C*, 2018, **122**, 16315–16324.

39 O. Sengul, E. B. Boydas, M. Pastore, W. Sharmouk, P. C. Gros, S. Catak and A. Monari, Probing optical properties of thiophene derivatives for two-photon absorption, *Theor. Chem. Acc.*, 2017, **136**, 67.

40 J. Sandland and R. W. Boyle, Photosensitizer Antibody–Drug Conjugates: Past, Present, and Future, *Bioconjugate Chem.*, 2019, **30**, 975–993.

41 V. Biju, Chemical modifications and bioconjugate reactions of nanomaterials for sensing, imaging, drug delivery and therapy, *Chem. Soc. Rev.*, 2014, **43**, 744–764.

42 M. J. Frisch, G. Trucks, H. B. Schlegel, G. E. Scuseria, M. A. Robb, J. R. Cheeseman, G. Scalmani, V. Barone, G. A. Petersson, H. Nakatsuji, X. Li, M. Caricato, A. V. Marenich, J. Bloino, B. G. Janesko, R. Gomperts, B. Mennucci and D. J. Hratch, *Gaussian 16, Rev. A.03*, Gaussian, Inc., Wallingford, CT, 2009.

43 G. Scalmani and M. J. Frisch, Continuous surface charge polarizable continuum models of solvation. I. General formalism, *J. Chem. Phys.*, 2010, **132**, 114110.

44 J. Tomasi, B. Mennucci and R. Cammi, Quantum Mechanical Continuum Solvation Models, *Chem. Rev.*, 2005, **105**, 2999–3094.

45 Y. Zhao and D. G. Truhlar, The M06 suite of density functionals for main group thermochemistry, thermochemical kinetics, noncovalent interactions, excited states, and transition elements: two new functionals and systematic testing of four M06-class functionals and 12 other fun, *Theor. Chem. Acc.*, 2008, **120**, 215–241.

46 S. J. Choe, Comparison of Different Theory Models and Basis Sets in DFT Comparison of Different Theory Models and Basis Sets in Calculations of TPOP24N-Oxide Geometry and Geometries of meso-Tetraphenyl Chlorin N-Oxide Regioisomers, *Korean Chem. Soc.*, 2012, **33**, 2861.

47 T. Yanai, D. P. Tew and N. C. Handy, A new hybrid exchange-correlation functional using the Coulomb-attenuating method (CAM-B3LYP), *Chem. Phys. Lett.*, 2004, **393**, 51–57.

48 Y. Tawada, T. Tsuneda, S. Yanagisawa, T. Yanai and K. Hirao, A long-range-corrected time-dependent density functional theory, *J. Chem. Phys.*, 2004, **120**, 8425–8433.

49 J. Da Chai and M. Head-Gordon, Long-range corrected hybrid density functionals with damped atom-atom dispersion corrections, *Phys. Chem. Chem. Phys.*, 2008, **10**, 6615–6620.

50 M. Barbatti, M. Ruckenbauer, F. Plasser, J. Pittner, G. Granucci, M. Persico, H. Lischka and J. Wiley, Newton-X: A surface-hopping program for nonadiabatic molecular

dynamics, *Wiley Interdiscip. Rev.: Comput. Mol. Sci.*, 2014, **4**, 26–33.

51 O. Sengul, E. Birsen, B. Mariachiara and W. Sharmouk, Probing optical properties of thiophene derivatives for two-photon absorption, *Theor. Chem. Acc.*, 2017, 1–9.

52 K. Aidas, C. Angeli, K. L. Bak, V. Bakken, R. Bast, L. Boman, O. Christiansen, R. Cimiraglia, S. Coriani, P. Dahle, E. K. Dalskov, U. Ekström, T. Enevoldsen, J. J. Eriksen, P. Ettenhuber, B. Fernández, L. Ferrighi, H. Fliegl, L. Frediani, K. Hald, A. Halkier, C. Hättig, H. Heiberg, T. Helgaker, A. C. Hennum, H. Hettema, E. Hjertenæs, S. Høst, I. M. Høyvik, M. F. Iozzi, B. Jansík, H. J. A. Jensen, D. Jonsson, P. Jørgensen, J. Kauczor, S. Kirpekar, T. Kjærgaard, W. Klopper, S. Knecht, R. Kobayashi, H. Koch, J. Kongsted, A. Krapp, K. Kristensen, A. Ligabue, O. B. Lutnæs, J. I. Melo, K. V. Mikkelsen, R. H. Myhre, C. Neiss, C. B. Nielsen, P. Norman, J. Olsen, J. M. H. Olsen, A. Osted, M. J. Packer, F. Pawlowski, T. B. Pedersen, P. F. Provasi, S. Reine, Z. Rinkevicius, T. A. Ruden, K. Ruud, V. V. Rybkin, P. Sałek, C. C. M. Samson, A. S. de Merás, T. Saue, S. P. A. Sauer, B. Schimmelpfennig, K. Sneskov, A. H. Steindal, K. O. Sylvester-Hvid, P. R. Taylor, A. M. Teale, E. I. Tellgren, D. P. Tew, A. J. Thorvaldsen, L. Thøgersen, O. Vahtras, M. A. Watson, D. J. D. Wilson, M. Ziolkowski and H. Ågren, The Dalton quantum chemistry program system, *Wiley Interdiscip. Rev.:Comput. Mol. Sci.*, 2014, **4**, 269–284.

53 M. Chołuj, M. M. Alam, M. T. P. Beerepoot, S. P. Sitkiewicz, E. Matito, K. Ruud and R. Zaleśny, Choosing Bad versus Worse: Predictions of Two-Photon-Absorption Strengths Based on Popular Density Functional Approximations, *J. Chem. Theory Comput.*, 2022, **18**, 1046–1060.

54 M. T. P. Beerepoot, M. M. Alam, J. Bednarska, W. Bartkowiak, K. Ruud and R. Zaleśny, Benchmarking the Performance of Exchange-Correlation Functionals for Predicting Two-Photon Absorption Strengths, *J. Chem. Theory Comput.*, 2018, **14**, 3677–3685.

55 T. Etienne, Probing the locality of excited states with linear algebra, *J. Chem. Theory Comput.*, 2015, **11**, 1692–1699.

56 T. Etienne, X. Assfeld and A. Monari, New insight into the topology of excited states through detachment/attachment density matrices-based centroids of charge, *J. Chem. Theory Comput.*, 2014, **10**, 3906–3914.

57 T. Etienne, X. Assfeld and A. Monari, Toward a quantitative assessment of electronic transitions charge-transfer character, *J. Chem. Theory Comput.*, 2014, **10**, 3896–3905.

58 M. D. Hanwell, D. E. Curtis, D. C. Lonie, T. Vandermeerschd, E. Zurek and G. R. Hutchison, Avogadro: An advanced semantic chemical editor, visualization, and analysis platform, *J. Cheminf.*, 2012, **4**, 1–17.

59 R. Rüger, M. Franchini, T. Trnka, A. Yakovlev, E. van Lenthe, P. Philipsen, T. van Vuren, B. Klumpers and T. Soini, *AMS 2022.1,* SCM, Theoretical Chemistry, Vrije Universiteit, Amsterdam, The Netherlands, 2022, **http://www.scm.com**.

60 R. Salomon-Ferrer, D. A. Case and R. C. Walker, An overview of the Amber biomolecular simulation package, **3**, 198–210.

61 D. A. Case, T. E. Cheatham, T. Darden, H. Gohlke, R. Luo, K. M. Merz, A. Onufriev, C. Simmerling, B. Wang and R. J. Woods, The Amber biomolecular simulation programs, 2005, preprint, DOI: **10.1002/jcc.20290**.

62 J. Wang, W. Wang, P. A. Kollman and D. A. Case, Automatic atom type and bond type perception in molecular mechanical calculations, *J. Mol. Graphics Modell.*, 2006, **25**, 247260.

63 J. Wang, R. M. Wolf, J. W. Caldwell, P. A. Kollman and D. A. Case, Development and testing of a general amber force field, *J. Comput. Chem.*, 2004, **25**, 1157–1174.

64 A. K. Schmidt, S. Cottaz, H. Driguez and G. E. Schulz, Structure of Cyclodextrin Glycosyltransferase Complexed with a Derivative of Its Main Product β-Cyclodextrin, *Biochemistry*, 1998, **37**, 5909–5915.

65 A. K. Schmidt, S. Cottaz, H. Driguez and G. E. Schulz, Structure of cyclodextrin glycosyltransferase complexed with a derivative of its main product β-cyclodextrin, *Biochemistry*, 1998, **37**, 5909–5915.

66 K. N. Kirschner, A. B. Yongye, S. M. Tschampel, J. Gonza, C. R. Daniels, B. L. Foley and R. J. Woods, GLYCAM06: A Generalizable Biomolecular Force Field, DOI: **10.1002/jcc**.

67 S. Jo, T. Kim, V. G. Iyer and W. Im, CHARMM-GUI: A web-based graphical user interface for CHARMM, *J. Comput. Chem.*, 2008, **29**, 1859–1865.

68 P. Mark and L. Nilsson, Structure and dynamics of the TIP3P, SPC, and SPC/E water models at 298 K, *J. Phys. Chem. A*, 2001, **105**, 9954–9960.

69 C. J. Dickson, R. C. Walker and I. R. Gould, Lipid21: Complex Lipid Membrane Simulations with AMBER, *J. Chem. Theory Comput.*, 2022, **18**, 1726–1736.

70 S. E. Feller, Y. Zhang, R. W. Pastor and B. R. Brooks, Constant pressure molecular dynamics simulation: The Langevin piston method, *J. Chem. Phys.*, 1995, **103**, 4613–4621.

71 H. J. C. Berendsen, J. P. M. Postma, W. F. Van Gunsteren, A. Dinola and J. R. Haak, Molecular dynamics with coupling to an external bath, *J. Chem. Phys.*, 1984, **81**, 3684–3690.

72 T. Darden, D. York and L. Pedersen, Particle mesh Ewald: An N log(N) method for Ewald sums in large systems, *J. Chem. Phys.*, 1993, **98**, 10089–10092.

73 C. W. Hopkins, S. Le Grand, R. C. Walker and A. E. Roitberg, Long-time-step molecular dynamics through hydrogen mass repartitioning, *J. Chem. Theory Comput.*, 2015, **11**(4), 1864–1874, DOI: **10.1021/ct5010406**.

74 J. P. Ryckaert, G. Ciccotti and H. J. C. Berendsen, Numerical integration of the cartesian equations of motion of a system with constraints: molecular dynamics of n-alkanes, *J. Comput. Phys.*, 1977, **23**, 327–341.

75 D. R. Roe and T. E. I. Cheatham, PTRAJ and CPPTRAJ: Software for Processing and Analysis of Molecular Dynamics Trajectory Data, *J. Chem. Theory Comput.*, 2013, **9**, 3084–3095.

76 D. A. Case, H. M. Aktulga, K. Belfon, D. S. Cerutti, G. A. Cisneros, V. W. D. Cruzeiro, N. Forouzesh,

T. J. Giese, A. W. Götz, H. Gohlke, S. Izadi, K. Kasavajhala, M. C. Kaymak, E. King, T. Kurtzman, T.-S. Lee, P. Li, J. Liu, T. Luchko, R. Luo, M. Manathunga, M. R. Machado, H. M. Nguyen, K. A. O'Hearn, A. V. Onufriev, F. Pan, S. Pantano, R. Qi, A. Rahnamoun, A. Risheh, S. Schott-Verdugo, A. Shajan, J. Swails, J. Wang, H. Wei, X. Wu, Y. Wu, S. Zhang, S. Zhao, Q. Zhu, T. E. I. Cheatham, D. R. Roe, A. Roitberg, C. Simmerling, D. M. York, M. C. Nagan and K. M. Merz, AmberTools, *J. Chem. Inf. Model.*, 2023, **63**, 6183–6191.

77 W. Humphrey, A. Dalke and K. Schulten, VMD: Visual molecular dynamics, *J. Mol. Graphics*, 1996, **14**, 33–38.

78 R. Guixà-González, I. Rodriguez-Espigares, J. M. Ramírez-Anguita, P. Carrió-Gaspar, H. Martinez-Seara, T. Giorgino and J. Selent, MEMBPLUGIN: studying membrane complexity in VMD, *Bioinformatics*, 2014, **30**, 1478–1480.

79 T. Giorgino, Computing 1-D atomic densities in macromolecular simulations: The density profile tool for VMD, *Comput. Phys. Commun.*, 2014, **185**, 317–322.

80 C. M. Isborn, A. W. Götz, M. A. Clark, R. C. Walker and T. J. Martínez, Electronic absorption spectra from MM and ab initio QM/MM molecular dynamics: Environmental effects on the absorption spectrum of photoactive yellow protein, *J. Chem. Theory Comput.*, 2012, **8**, 5092–5106.

81 L. Wu, J. Liu, P. Li, B. Tang and T. D. James, Two-photon small-molecule fluorescence-based agents for sensing, imaging, and therapy within biological systems, *Chem. Soc. Rev.*, 2025, **50**(2), 702–734.

82 S. Achelle, P. Couleaud, P. Baldeck, M.-P. Teulade-Fichou and P. Maillard, Carbohydrate-Porphyrin Conjugates with Two-Photon Absorption Properties as Potential Photosensitizing Agents for Photodynamic Therapy, *Eur. J. Org. Chem.*, 2011, 1271–1279.

83 H. Gattuso, E. Dumont, M. Marazzi and A. Monari, Two-photon-absorption DNA sensitization: Via solvated electron production: Unraveling photochemical pathways by molecular modeling and simulation, *Phys. Chem. Chem. Phys.*, 2016, **18**, 18598–18606.

84 H. Gattuso, A. Monari and M. Marazzi, Photophysics of chlorin e6: from one- and two-photon absorption to fluorescence and phosphorescence, *RSC Adv.*, 2017, **7**(18), 10992–10999.

85 F. Hammerer, G. Garcia, S. Chen, F. Poyer, S. Achelle, C. Fiorini-Debuisschert, M.-P. Teulade-Fichou and P. Maillard, Synthesis and Characterization of Glycoconjugated Porphyrin Triphenylamine Hybrids for Targeted Two-Photon Photodynamic Therapy, *J. Org. Chem.*, 2014, **79**, 1406–1417.

86 T. Ishi-I, Y. Taguri, S. I. Kato, M. Shigeiwa, H. Gorohmaru, S. Maeda and S. Mataka, Singlet oxygen generation by two-photon excitation of porphyrin derivatives having two-photon-absorbing benzothiadiazole chromophores, *J. Mater. Chem.*, 2007, **17**, 3341–3346.

87 M. E. Alberto, T. Marino, A. D. Quartarolo and N. Russo, Photophysical origin of the reduced photodynamic therapy activity of temocene compared to Foscan®: Insights from theory, *Phys. Chem. Chem. Phys.*, 2013, **15**, 16167–16171.

88 L. Xu, J. Chai, Y. Wang, X. Zhao, D.-S. Guo, L. Shi, Z. Zhang and Y. Liu, Calixarene-integrated nano-drug delivery system for tumor-targeted delivery and tracking of anti-cancer drugs in vivo, *Nano Res.*, 2022, **15**, 7295–7303.

